Hindawi Publishing Corporation
International Journal of Photoenergy
Volume 2012, Article ID 703496, 7 pages
doi:10.1155/2012/703496

Research Article

White Organic Light-Emitting Diodes Using Two Phosphorescence Materials in a Starburst Hole-Transporting Layer

Tomoya Inden,[1] Tomoya Hishida,[2] Masayuki Takahashi,[2] Masato Ohsumi,[2] and Naoki Ohtani[2]

[1] *Graduate School of Engineering, Nagoya University, Furo-cho, Chikusa-ku, Nagoya 464-8603, Japan*
[2] *Department of Electronics, Doshisha University, 1-3 Tatara-Miyakodani, Kyotanabe, Kyoto 610-0321, Japan*

Correspondence should be addressed to Naoki Ohtani, ohtani@mail.doshisha.ac.jp

Received 15 June 2011; Revised 14 October 2011; Accepted 28 October 2011

Academic Editor: Jimmy Yu

We fabricated two kinds of white organic light-emitting diodes (WOLEDs); one consisted of two emissive materials of red and blue, and the other of three emissive materials of red, green, and blue. The red and blue emissive materials were phosphorescent. We evaluated the thickness dependence of the CIE coordinate, the external quantum efficiency (EQE), and the luminance by changing the thicknesses of the Ir(btp)2acac and FIrpic layers. Samples consisting of three emissive materials revealed the best CIE coordinate and the best EQE in the same sample structure. On the other hand, the samples consisting of two emissive materials revealed the best CIE coordinate and the best EQE in different structures. The best CIE coordinate of (0.33, 0.36) was observed by changing the thicknesses of the stacked active layers. The best EQE was 9.73%, which was observed in the sample consisting of different thickness of stacked active layers.

1. Introduction

Research on organic light-emitting diodes (OLEDs) has been attracting much interest for applications to full-color flat-panel displays and illumination light sources. In particular, white OLEDs (WOLEDs) are the candidate for novel illumination light sources. However, WOLEDs should be improved in their efficiency and operating lifetime for practical use. To solve these problems, most of the recent research on WOLEDs has used phosphorescent emissive materials instead of fluorescent ones. These days the highest external quantum efficiency (EQE) of green emission using phosphorescent material exceeds 20% [1].

WOLEDs can be fabricated by two methods. The most common method is using three primary color emissive materials in an emitting layer (EML). Sun et al. [2] reported that a hybrid WOLED with a fluorescent blue emitter and phosphorescent red and green emitters showed the highest EQE of 18.7%. Another method to make white emission only uses two complimentary colors.

In this paper, we fabricated two kinds of WOLEDs. One consists of two emissive materials of red and green, and the other consists of three emissive materials of red, green, and blue. The former is called an RGB-type sample, and the latter one is an RB-type sample. The red and blue emissive materials are phosphorescent materials. [Bis(2-(2′-benzothienyl)pyridinato-N,$C^{3'}$)iridium(acetylacetonate)] (Ir(btp)2acac) is used as a red emissive phosphorescent material, and [Bis (4,6-difluorophenylpyridinato-N,C^{2})picolinatoiridium] (FIrpic) is used as a blue emissive phosphorescent material. In addition, [Tris (8-hydroxyquinolinato)-aluminum] (Alq3) is used as a green emissive and electron-transporting fluorescent material. We evaluated the thickness dependence on the CIE coordinate, the external quantum efficiency, and the luminance by changing the thicknesses of the Ir(btp) 2acac and FIrpic layers.

2. Experimental Procedure and Sample Structures

2.1. Organic Materials. Figures 1 and 2 show the energy band diagram of the RGB- and RB-type samples. The HOMO-LUMO values are estimated from [3].

[Dicarbazolyl-3,5-benzene] (MCP) can be used as a host material in the emitting layers because it has a higher triplet energy than FIrpic. In previous studies, [4,4′-Bis(N-carbazolyl)-1,1′-biphenyl] (CBP) has usually been used as the host material of green or red phosphorescent materials because CBP has higher triplet energy than they do [4]. Its triplet energy, however, is lower than FIrpic, indicating that EQE cannot be improved by combining CBP and FIrpic. Thus, we use MCP as the host material in both the Ir(btp)2acac and FIrpic layers.

In RGB-type samples, the Alq3 layer is an electron-transporting layer (ETL), and [2,9-Dimethyl-4,7-diphenyl-1,10-phenanthroline] (BCP) is used as an ETL in the RB-type samples. In addition, [4,4′,4″-tris-(3-methylphenylphenylamino) triphenylamine] (m-MTDATA) is used as a hole-transporting layer on the ITO electrode in both types of samples. m-MTDATA also works as an electron-blocking layer. In addition, the discontinuity of the HOMO levels of m-MTDATA and FIrpic play a role in hole blocking, improving the radiative efficiency.

In the RB-type samples, we caused a radiative recombination in the FIrpic layer because the discontinuity of the HOMO levels between BCP and FIrpic works as a hole-blocking interface.

2.2. Sample Fabrication. The organic materials were deposited on sufficiently cleaned ITO-coated glass substrate by using a vacuum evaporator. The pressure was under 3×10^{-4} Pa, and the deposition rates of the HTL and the ETL were between 0.1 and 0.2 nm/s and were monitored with a quartz oscillator. After deposition of all the organic materials, LiF and Al were deposited as a cathode. The mesa area was 4 mm^2.

The following are the sample structures of the RGB type and RB type:
RGB type:

(A) ITO/m-MTDATA/FIrpic + MCP(25 nm)/Ir(btp)2acac + MCP(5 nm)/Alq3/LiF/Al:

deposition rate of FIrpic was between 0.1 and 0.3 nm/s,
deposition rate of Ir(btp)2acac was between 0.1 and 0.2 nm/s,
average doping density of FIrpic was 10 mol%, and average doping density of Ir(btp)2acac was 10 mol%.

(B) ITO/m-MTDATA/FIrpic + MCP(25 nm)/Ir(btp)2acac + MCP(5 nm)/Alq3/LiF/Al:

deposition rate of FIrpic was between 0.3 and 0.5 nm/s,
deposition rate of Ir(btp)2acac was between 0.1 and 0.2 nm/s,
average doping density of FIrpic was 20 mol%, and
average doping density of Ir(btp)2acac was 10 mol%;

(C) ITO/m-MTDATA/FIrpic + MCP(20 nm)/Ir(btp)2acac + MCP(5 nm) /FIrpic + MCP(5 nm)/ Alq3/LiF/Al:

deposition rate of FIrpic was between 0.1 and 0.3 nm/s,
deposition rate of Ir(btp)2acac was between 0.1 and 0.2 nm/s,
average doping density of FIrpic was 10 mol%, and
average doping density of Ir(btp)2acac was 10 mol%;

RB type:

(D) ITO/m-MTDATA/Ir(btp)2acac + MCP(5 nm)/FIrpic + MCP(25 nm)/BCP/LiF/Al:

deposition rate of FIrpic was between 0.1 and 0.3 nm/s,
deposition rate of Ir(btp)2acac was between 0.1 and 0.2 nm/s,
average doping density of FIrpic was 10 mol%, and
average doping density of Ir(btp)2acac was 10 mol%;

(E) ITO/m-MTDATA/Ir(btp)2acac + MCP(5 nm)/FIrpic + MCP(25 nm)/BCP/LiF/Al:

deposition rate of FIrpic was between 0.3 and 0.5 nm/s,
deposition rate of Ir(btp)2acac was between 0.1 and 0.2 nm/s,
average doping density of FIrpic was 20 mol%, and
average doping density of Ir(btp)2acac was 10 mol%;

(F) ITO/m-MTDATA/Ir(btp)2acac + MCP(1 nm)/FIrpic + MCP(29 nm)/BCP/LiF/Al:

deposition rate of FIrpic was between 0.1 and 0.3 nm/s,
deposition rate of Ir(btp)2acac was between 0.1 and 0.2 nm/s,
average doping density of FIrpic was 10 mol%, and
average doping density of Ir(btp)2acac was 10 mol%;

(G) ITO/m-MTDATA/Ir(btp)2acac + MCP(1 nm)/FIrpic + MCP(29 nm)/BCP/LiF/Al:

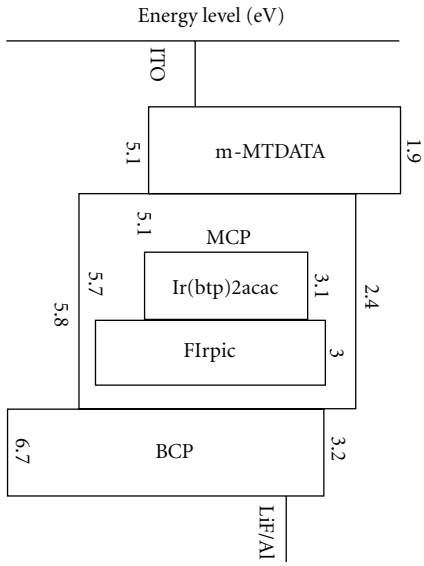

Figure 1: Energy diagram in all RGB-type samples.

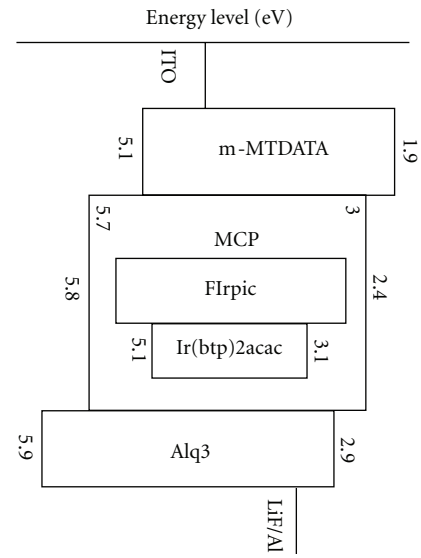

Figure 2: Energy diagram in all RB-type samples.

deposition rate of FIrpic was between 0.3 and 0.5 nm/s,

deposition rate of Ir(btp)2acac was between 0.1 and 0.2 nm/s,

average doping density of FIrpic was 20 mol%, and

average doping density of Ir(btp)2acac was 10 mol%,

deposition rate of MCP was fixed between 2.0 and 2.3 nm/s in all samples.

We evaluated the current-voltage (I-V) characteristics, the EQEs, the current density-luminance (J-L) characteristics, the CIE coordinates, and the EL spectra. The I-V characteristics were measured with a semiconductor parameter analyzer (4155C, Agilent Technologies). The luminance and the EL spectra of all the samples and the photons per unit of time were measured with an integrating sphere connected CCD spectrophotometer (USB 2000, Ocean Optics). The CIE coordinates were measured with a color-luminance meter (CS-100A, KONIKA MINOLTA). All measurements were performed in air.

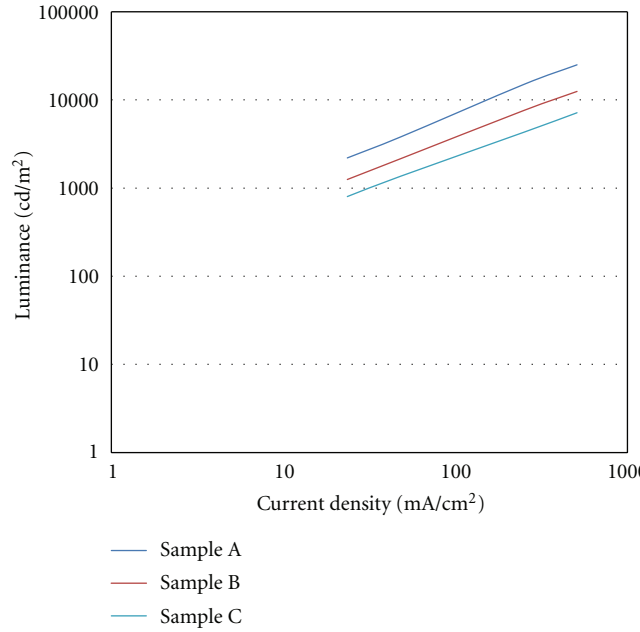

Figure 3: J-L characteristics in all RGB-type samples.

3. Results and Discussion

3.1. RGB-Type Samples. Figure 3 shows the J-L characteristics of the RGB-type samples. This result clearly shows that the luminance becomes lower with an increase of doping density. This is most likely caused by concentration quenching. In addition, the gradients of the J-L characteristics in the three samples is almost equal, because the relation between the current density and the disappearance of the photons are almost equal. When the value of the applied voltage is between 0 and 18 V, sample A shows a maximum luminance of 39500 cd/m^2. On the other hand, sample B shows a maximum luminance of 20300 cd/m^2 with the same applied voltage.

Figure 4 shows the J-EQE characteristics of the RGB-type samples. The measurement range of the current density is between 25 and 1250 mA/cm^2. When the current density is less than 25 mA/cm^2, the photon counting does not work due to a lack of photons. The EQE in sample A is larger than the others due to the large concentration quenching in samples B and C. With increasing current density, the EQE in the three samples sharply decreases. This is attributed to the effect of the triplet-triplet annihilation (T-T annihilation) in the large

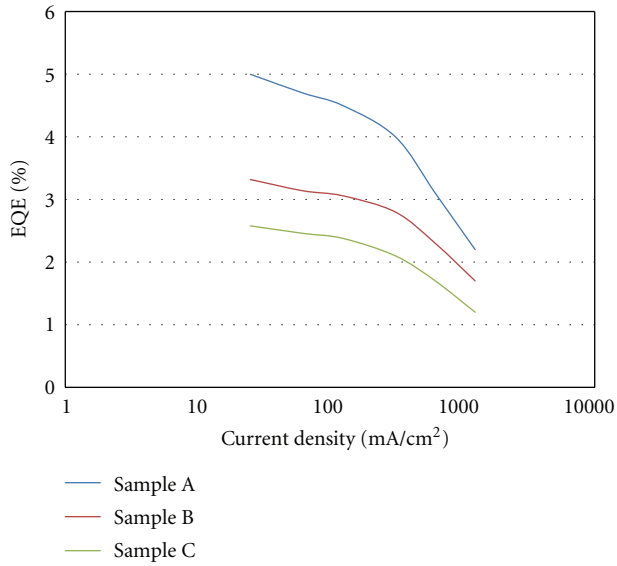

Figure 4: J-EQE characteristics in all RGB-type samples.

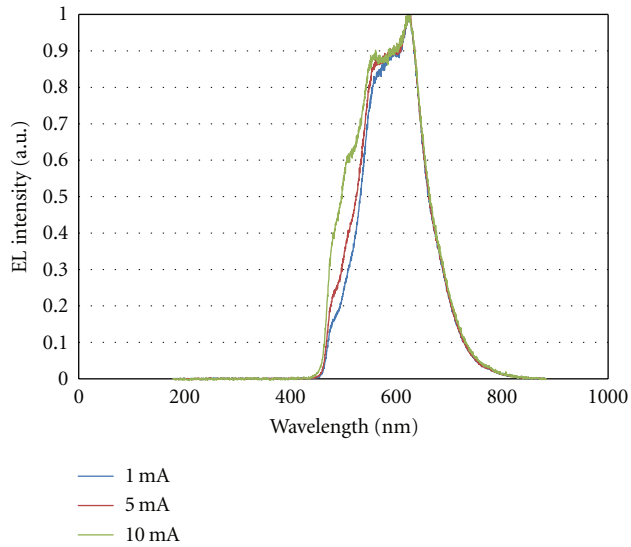

Figure 5: EL spectra in sample A. Injected currents are 1, 5, and 10 mA.

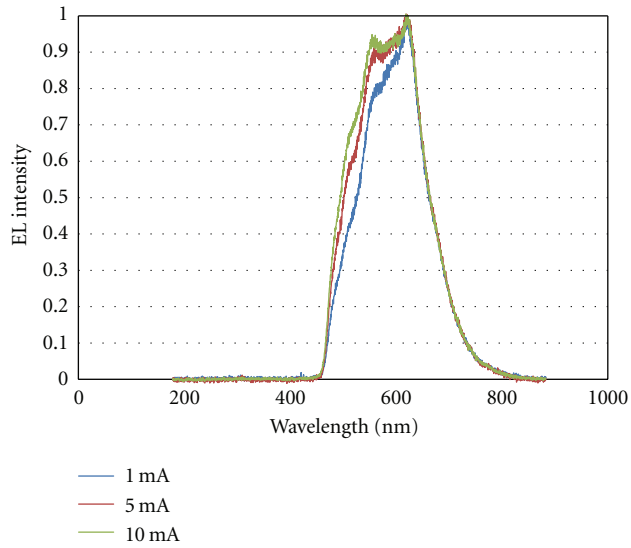

Figure 6: EL spectra in sample B. Injected currents are 1, 5, and 10 mA.

current density region. T-T annihilation means the disappearance of the triplet excitons, which occurs when their density in the emitting layers becomes very large [5].

Table 1 shows the CIE coordinate in the RGB-type samples. The best white emission is observed in sample A. The CIE coordinate is (0.33, 0.41). The nearest white coordinate in sample B is (0.35, 0.44). Compared with sample A, sample B's CIE coordinate is slightly red shifted at the same current. In addition, the CIE coordinates of both samples are blue shifted with increasing current density, indicating that the radiative recombination region is changed to wider-bandgap material.

The operating property in sample C is the worst of the RGB-type samples. The best white coordinate in sample C is (0.38, 0.46). Compared with the others, the CIE coordinate shows a red shift. This means that the radiative recombination occurs mainly in the Ir(btp)2acac layer due to the narrow bandgap. Thus, many triplet excitons gather in the Ir(btp)2acac layer, leading to T-T annihilation as well as the decrease of luminance and EQE.

Finally, Figures 5, 6, and 7 show the EL spectra of all the RGB-type samples. The EL intensities are normalized at the intensity of Ir(btp)2acac. The EL intensities of both FIrpic and Alq3 in sample A are stronger than those of both FIrpic and Alq3 in sample B. This means that the EL spectrum in sample A is wider than that in sample B. Therefore, the CIE coordinate in sample A is better for generating white color emission. In addition, the EL intensities of both FIrpic and Alq3 in sample C are small and result in the red shift of the CIE coordinate.

We evaluated the EL spectra of the three samples at the same currents of 1, 5, and 10 mA. The EL spectrum of every RGB-type sample depends on the applied voltage. In particular, with an increase of the applied voltage, the EL intensity from the Ir(btp)2acac layer becomes weaker, while the EL intensity from Alq3 becomes stronger. However, the EL emissions from the three primary colors can always be observed within the range of every applied voltage. This means that the energy transfer is not caused by the applied voltage; the radiative recombination occurs in the same emitting layers.

These results concerning to the RGB-type samples clearly demonstrate that the best CIE coordinate and the best EQE are observed in sample A.

3.2. RB-Type Samples. Figure 8 shows the J-L characteristics of the RB-type samples. Samples E and G containing larger doping densities reveal smaller luminance than samples D and F. This is also caused by concentration quenching. In addition, the gradients of the J-L characteristics in the same

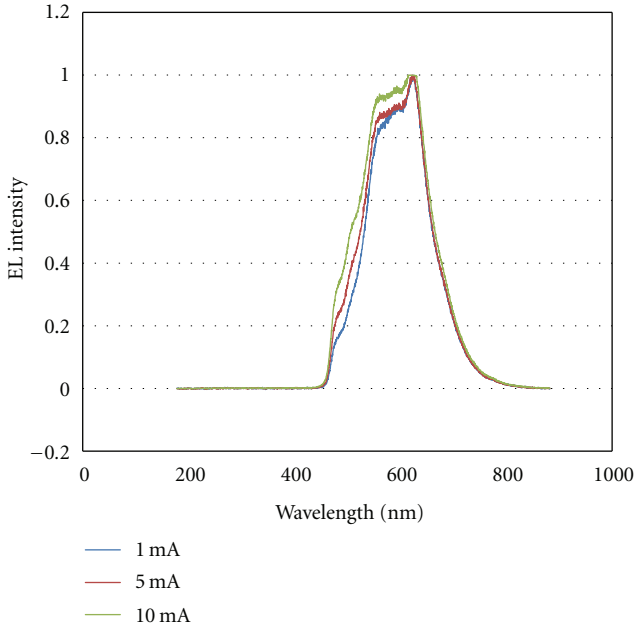

Figure 7: EL spectra in sample C. Injected currents are 1, 5, and 10 mA.

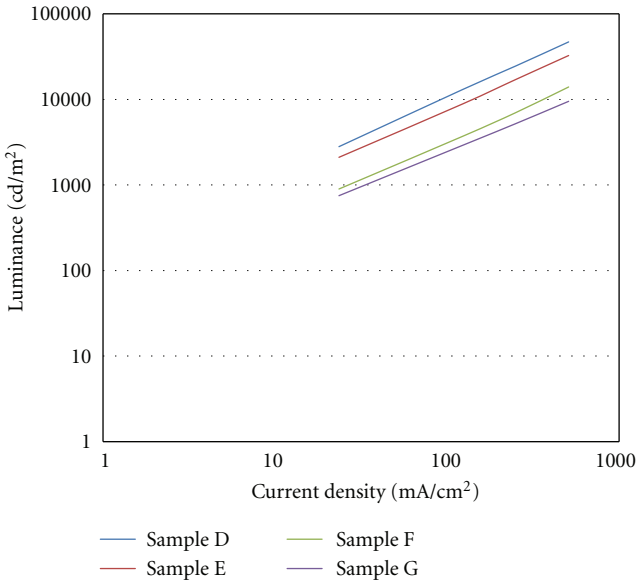

Figure 8: J-L characteristics in all RB-type samples.

Table 1: CIE coordinate in all RGB-type samples.

	Current (mA)			
Sample	1	5	10	20
A	(0.37, 0.48)	(0.35, 0.45)	(0.33, 0.41)	(0.33, 0.42)
B	(0.40, 0.46)	(0.36, 0.46)	(0.35, 0.45)	(0.35, 0.44)
C	(0.45, 0.49)	(0.45, 0.48)	(0.43, 0.45)	(0.38, 0.46)

sample structures are almost equal. This result is similarly observed in the RGB-type samples, meaning that the relation

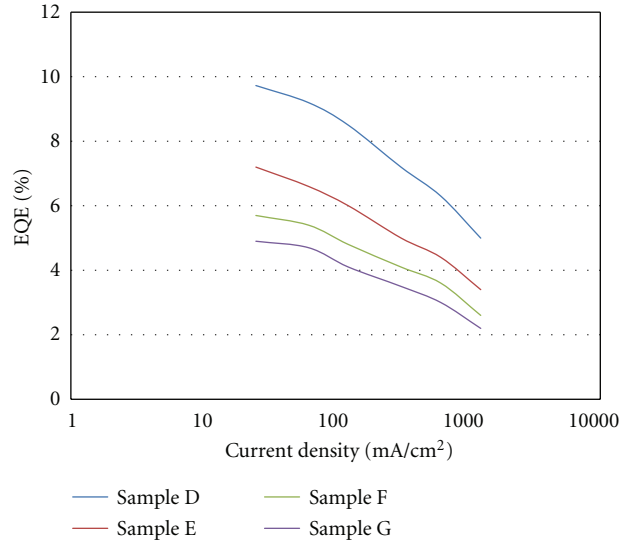

Figure 9: J-EQE characteristics in all RB-type samples.

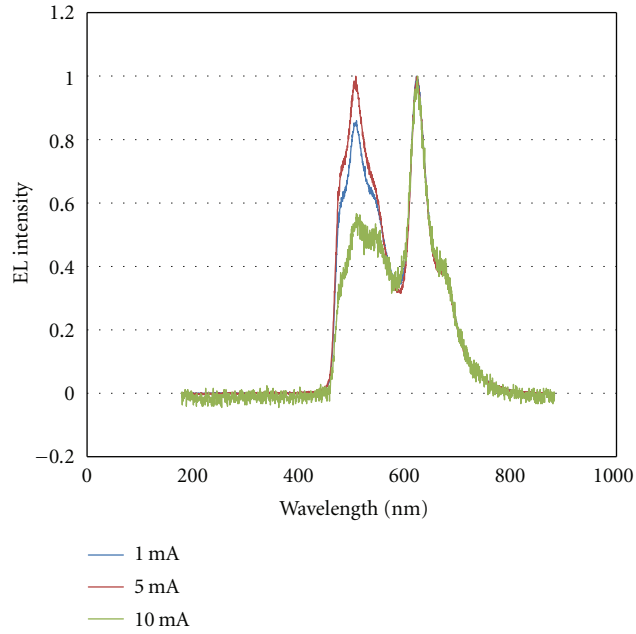

Figure 10: EL spectra in sample D. Injected currents are 1, 5, and 10 mA.

between the current density and the disappearance of the photons is almost equal when the sample structure is identical. When the range of the applied voltage is between 0 and 18 V, the maximum luminance shows 71135 cd/m^2 in sample D. The second highest maximum luminance shows 48108 cd/m^2 in sample F with the same applied voltage.

Figure 9 shows the J-EQE characteristics in all the RB-type samples. The injected current densities are the same as the RGB-type. The EQEs of all four samples increase with decreasing current density, because EQE is proportional to the amount of photons and inversely proportional to the current density.

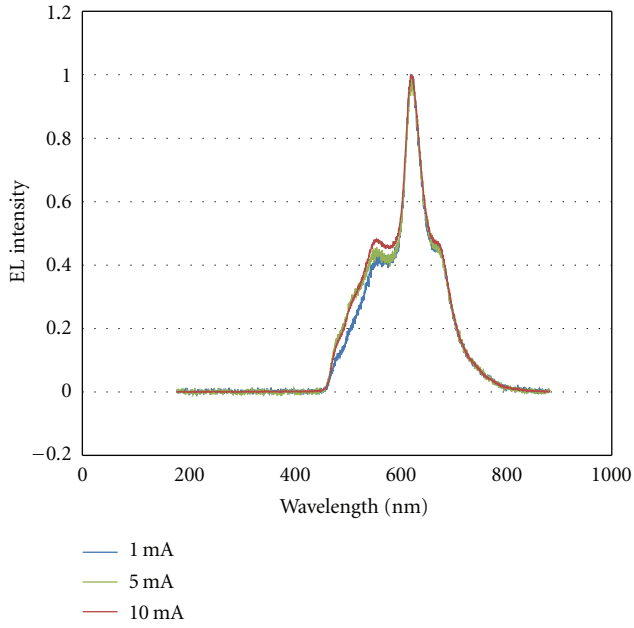

Figure 11: EL spectra in sample E. Injected currents are 1, 5, and 10 mA.

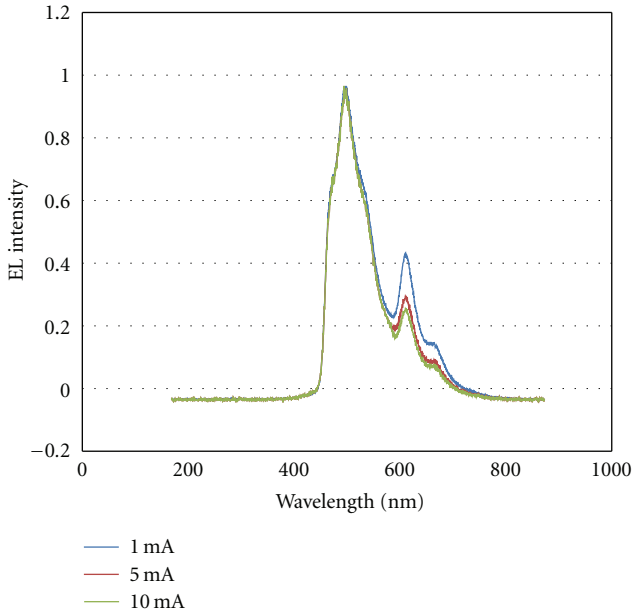

Figure 12: EL spectra in sample F. Injected currents are 1, 5, and 10 mA.

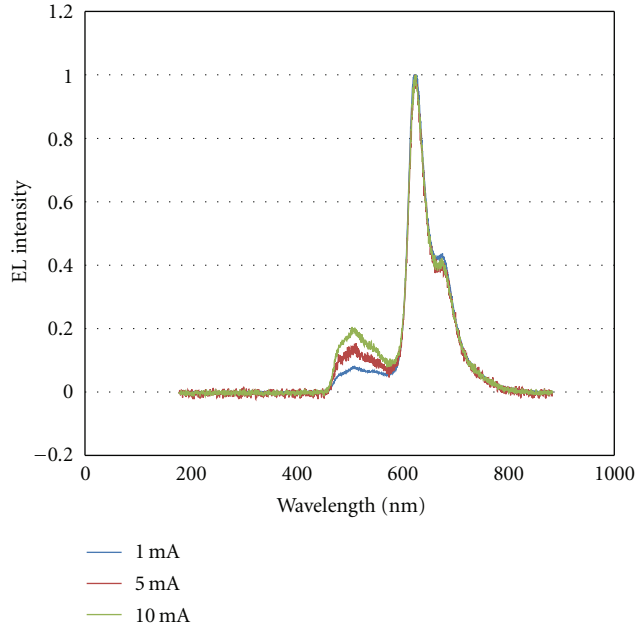

Figure 13: EL spectra in sample G. Injected currents are 1, 5, and 10 mA.

Table 2: CIE coordinate in all RB-type samples.

	Current (mA)			
Sample	1	5	10	20
D	(0.45, 0.40)	(0.37, 0.38)	(0.34, 0.49)	(0.31, 0.38)
E	(0.48, 0.48)	(0.45, 0.46)	(0.44, 0.46)	(0.45, 0.43)
F	(0.38, 0.36)	(0.33, 0.36)	(0.31, 0.39)	(0.30, 0.38)
G	(0.38, 0.40)	(0.36, 0.40)	(0.34, 0.40)	(0.34, 0.39)

Sample D shows the maximum EQE of the RB-type samples, which is 9.73%. This sample is the most efficient among the RB type.

When the doping density of FIrpic is changed between 10 and 20 mol%, the range of the decrease of EQE is almost equal among the same sample structures. This indicates that the decrease of luminance due to concentration quenching depends on the doping density. In addition, the decrease of EQE among the large current density region is caused by T-T annihilation. Thus, the concentration quenching and T-T annihilation enter at the same time from a certain current density region.

To consider the influence of the Ir(btp)2acac layer thickness, we compared the luminance and EQE properties between samples D and F and samples E and G. The samples consisting of a 5 nm Ir(btp)2acac layer reveal better luminance and EQE properties than those consisting of a 1-nm Ir(btp)2acac layer. Since the discontinuity of the HOMO levels of Ir(btp)2acac layer and FIrpic layer is 0.6 eV as shown in Figure 2, many holes are trapped at the interface. Thus, higher luminance and the EQE in the samples D and F were actively caused by the recombination of the carriers between the Ir(btp)2acac layer and FIrpic layer. The ultrathin Ir(btp)2acac layer entered the separation of the careers between the Ir(btp)2acac and FIrpic layer (Figure 2). The small luminance and the EQE observed in samples E and G can be attributed to the increase of the nonradiative indirect transition due to the ultrathin Ir(btp)2acac layer. Table 2 shows the CIE coordinate in all the RB-type samples. The best white color emission is observed in sample F. The CIE coordinate was (0.33, 0.36). The second best white coordinate is observed in sample D, which reveals the highest luminance. All the RB-type samples similarly show a blue shift, indicating

that the recombination region partially moved to the FIrpic layer.

Figures 10, 11, 12, and 13 show the EL spectra in all the RB-type samples. The EL intensity of FIrpic is stronger than Ir(btp)2acac in samples D and F, reflecting weak concentration quenching. Thus, the emitting color in all the RB-type samples depends on the thickness of Ir(btp)2acac and the doping density in the EML materials.

The profile of the EL spectra depends on the applied oltage. With an increase of the applied voltage, the EL intensity from Ir(btp)2acac layer becomes weaker, and the EL intensity from FIrpic becomes relatively strong. This means that the carriers in the Ir(btp)2acac layer move to the adjacent wide-bandgap material FIrpic due to the change of the carrier mobility by the large applied voltage.

4. Conclusions

We fabricated and evaluated two kinds of WOLEDs. The luminance and EQE of both RGB- and RB-type samples were found to depend on the doping density and the T-T annihilation. For the RB-type samples, the thickness of the Ir(btp)2acac layer strongly affected the luminance and the EQE properties. The RGB-type samples exhibit the best CIE coordinate and the best EQE in the same sample structure; the best CIE coordinate was (0.34, 0.39), the maximum EQE was 9.73%, and the maximum luminance was 71135 cd/m^2. The RB-type samples exhibit the best CIE coordinate and the best EQE in different structures; the best CIE coordinate was (0.33, 0.36), the maximum EQE was 7.46%, and the maximum luminance was 48108 cd/m^2. The EQE can exceed 10% by a current injection less than 25 mA/cm^2 using five organic materials. This means that high performance white OLEDs can be fabricated using a few organic materials and simple sample structures.

References

[1] M. A. Baldo, S. Lamansky, P. E. Burrows, M. E. Thompson, and S. R. Forrest, "Very high-efficiency green organic light-emitting devices based on electrophosphorescence," *Applied Physics Letters*, vol. 75, no. 1, pp. 4–6, 1999.

[2] Y. Sun, N. C. Giebink, H. Kanno, B. Ma, M. E. Thompson, and S. R. Forrest, "Management of singlet and triplet excitons for efficient white organic light-emitting devices," *Nature*, vol. 440, no. 7086, pp. 908–912, 2006.

[3] X. Zhu, J. Sun, X. Yu, M. Wong, and H. S. Kwok, "High-performance top-emitting white organic light-emitting devices," *Japanese Journal of Applied Physics, Part 1*, vol. 46, no. 7, pp. 4054–4058, 2007.

[4] S. H. Kim, J. Jang, and J. Y. Lee, "Improved color stability in white phosphorescent organic light-emitting diodes using charge confining structure without interlayer," *Applied Physics Letters*, vol. 91, no. 12, Article ID 123509, 3 pages, 2007.

[5] M. A. Baldo, C. Adachi, and S. R. Forrest, "Transient analysis of organic electrophosphorescence. II. Transient analysis of triplet-triplet annihilation," *Physical Review B*, vol. 62, no. 16, pp. 10967–10977, 2000.